Diffusion behavior of iodine in the micro/nano-porous graphite for nuclear reactor at high temperature

Mingbo Qi , Pengfei Lian , Pengda Li , Heyao Zhang , Jinxing Cheng , Qingbo Wang , Zhongfeng Tang , T. J. Pan * , Jinliang Song * , Zhanjun Liu *

Posted Date: 19 July 2023

doi: 10.20944/preprints202307.1246.v1

Keywords: Micro/nano-porous graphite; Iodine, Fission products; Diffusion, High temperature; Rutherford backscattering spectrometry

Article

Diffusion Behavior of Iodine in the Micro/Nano-Porous Graphite for Nuclear Reactor at High Temperature

Ming-bo Qi[a,c†], Peng-fei Lian[b,e†], Peng-da Li[c,e], He-yao Zhang[a], Jin-xing Cheng[d], Qing-bo Wang[d], Zhong-feng Tang[c,f], T. J. Pan[a,*], Jin-liang Song[c,f*] and Zhanjun Liu[b,f*]

[a] School of Materials Science and Engineering, Changzhou University, Changzhou 213164, China;
[b] Key Laboratory of Carbon Materials, Institute of Coal Chemistry, Chinese Academy of Sciences, Taiyuan 030001, China;
[c] Shanghai Institute of Applied Physics, Chinese Academy of Sciences, Shanghai 201800, China;
[d] Beijing High-tech Institute, Beijing 100094, China;
[e] University of Chinese Academy of Sciences, Beijing 100049, China;
[f] Dalian National Laboratory for Clean Energy, Dalian 116023, China.
* Correspondence: author: T. J. Pan, Zhan-jun Liu and Jin-liang Song; Tel/Fax: +86-21-39194681; Email: tjpan@cczu.edu.cn&zjliu03@sxicc.ac.cn&jlsong1982@yeah.net
† The two authors contributed equally to this study and share first authorship.

Abstract: Using analysis methods such as Rutherford backscattering Spectrometry, scanning electron microscopy, X-ray diffraction, and Raman spectroscopy, the diffusion behavior of iodine in micro/nano-porous graphite under high-temperature conditions was studied. The results indicate that iodine diffusion leads to the contraction of graphite microcrystals, a decrease in interlayer spacing, and an increase in defect density, resulting in a reduction in microcrystal size. Upon diffusion of iodine out of iodine-loaded graphite, the microcrystal size of the graphite increases, the interlayer spacing appears to return to the initial state, and the defect density decreases. By comparing the iodine diffusion performance of nanoporous graphite G400 and G450 with microporous graphite G500, it was determined that nanoporous graphite exhibits better inhibition of iodine diffusion compared to microporous graphite. Studying the diffusion behavior of iodine in micro/nano-porous graphite has significant academic significance and engineering value for the screening, design, and performance optimization of nuclear graphite.

Keywords: micro/nano-porous graphite; iodine; fission products; diffusion; high temperature; rutherford backscattering spectrometry

1. Introduction

Diffusion of radioactive isotopes of iodine, particularly ^{131}I, in High-Temperature Gas-cooled Reactors (HTGRs) deserves attention both during normal operation and accident scenarios. When acquiring experience on iodine diffusion behavior in such reactors, the diffusion mechanisms between iodine and core materials must be taken into account[1]. This is crucial for assessing the durability of core materials and optimizing their performance. Graphite, which serves as both a moderator and structural material, is a key material in HTGR cores[2]. Investigating the diffusion behavior of iodine in graphite holds significant scientific importance for reactor design. Given the current development of graphite products, structurally dense, small-pored, and uniform graphite materials such as G400, G450, and G500 are potential candidates for various HTGR designs. This paper mainly analyzes the diffusion behavior of iodine in micro/nano-porous graphite at high temperatures.

Currently, the diffusion behavior of iodine in graphite has not been well characterized. Between 1976 and 1997, Muller reported on the migration of iodine in A3 matrix graphite during normal operation of HTGRs, describing the mechanisms of iodine diffusion through pores or graphite particle diffusion and further explaining that the rapid release of iodine from graphite is due to fast transport through the pores[3,4]. However, due to limitations in graphite manufacturing technology at

 doi:10.20944/preprints202307.1246.v1

that time, the graphitization degree of A3 matrix graphite was relatively low and did not meet the design requirements of HTGRs. On the other hand, IG-110 graphite with an average pore size of 2 μm has become an ideal candidate material for reactors due to its higher graphitization degree, high temperature stability, strength and stiffness, low thermal expansion coefficient, and corrosion resistance. Therefore, Carter[5,6] tested the diffusion coefficients of I^- and I_2 in bulk IG-110 graphite and compacted IG-110 graphite using ICP-MS, and the results showed that there was no significant difference in iodine diffusion coefficients between bulk IG-110 and compacted IG-110 graphite, both at the order of 10-10. They further described the low sensitivity of iodine diffusion to graphite pore size. In addition, Mukhawana[1] reported on the behavior of iodine injected into heat-treated highly oriented pyrolytic graphite (HOPG), where the results indicated an increased iodine loss rate with higher temperature heat treatment. Although there have been some reports on the migration and diffusion of iodine in graphite, there is still a lack of a systematic understanding of iodine diffusion behavior in graphite, particularly in micro/nano-porous graphite.

In this work, micro/nano-porous graphite G400, G450, and G500 with average pore sizes of 23 nm, 18 nm, and 553 nm, respectively, were used as the subjects for diffusion experiments. Iodine vapor at 650°C was employed as the diffusion source. The diffusion behavior of iodine in micro/nano-porous graphite was investigated using Rutherford Backscattering Spectrometry (RBS), Scanning Electron Microscopy (SEM), X-ray Diffraction (XRD), and Raman spectroscopy. The aim was to elucidate the diffusion mechanisms of iodine in micro/nano-porous graphite and to provide important scientific insights for the screening, design, and optimization of nuclear graphite materials.

2. Experimental

2.1. Sample preparation

Diffusion behavior of iodine in micro/nano-porous graphite were investigated by iodine vapor diffusion method. A series of micro/nano-porous graphite as research objects include both nanoporous graphite G400 and G450, as well as microporous graphite G500. The micro/nano-porous graphite derived from the mixtures of coal-tar pitch, natural graphite flake (NGF) and tetrahydrofuran were prepared by a liquid-phase mixing process according to our previous work. G400, G450 and G500 were named according to calcination temperature of the calcined mixed materials (calcined mixed material equivalent to coke). The average pore size of G400 and G450 is 23 nm and 18 nm, respectively, while the average pore size of G500 is 553 nm. Properties of micro/nano-porous graphite such as density, porosity or graphitization of fine-grained graphite are shown in Table 1. In this work, micro/nano-porous graphite G400, G450 and G500 were cut and ground into rectangular sheets with a size of 7.0 × 7.0 × 1.0 mm^3. The instruments and operations used for cutting and polishing all samples in this experiment were kept consistent to minimize experimental errors. The processed rectangular graphite sheets were repeatedly rinsed through anhydrous ethanol and deionized water, and then dried for iodine diffusion experiments.

Table 1. Properties of fine-grained graphite.

Properties	G400	G450	G500
Apparent density (g/cm^3)	1.76±0.02	1.77±0.02	1.84±0.02
Graphitization degree (%)	91.5±*0.2*	92.0±*0.2*	93.8±*0.2*
Average pore size (volume, nm)	23	18	553
Open porosity (%)	17.8±0.1	17.3±0.1	12.8±0.1

2.2. Diffusion experiment

In this work, the iodine was purchased from Sinopharm Chemical Reagent Co., Ltd. with a purity of ⩾99.99% and a total number of magazine cations ⩽0.01%. The details of the iodine diffusion experiment are described below. First, Iodine pellets (mass of about 0.40 g) were placed into dehydroxylated quartz tubes (the purpose of high temperature annealing of quartz tubes is to remove

Preprints (www.preprints.org) | NOT PEER-REVIEWED | Posted: 19 July 2023 doi:10.20944/preprints202307.1246.v1

the hydroxyl groups from the quartz tubes themselves to prevent them from affecting the experiment). And the processed 7.0×7.0×1.0 mm^3 micro/nano-porous graphite samples G400, G450 and G500 were immediately packed into quartz tubes. Then the quartz tubes were placed on a vacuum sealer for sealing and packing, while the air was removed from the quartz tubes. At the same time, the vacuum inside the sealed quartz tube is 0.15 Pa. Next, the above steps were repeated until the G400, G450 and G500 graphite were sealed in three quartz tubes, respectively. It is worth noting that the purpose of maintaining a vacuum inside the quartz tubes is to reduce the interference of airborne components in the work, especially oxygen and water. Finally, the quartz tube loaded with graphite and iodine was placed in GSL-1700X-HV high vacuum tube furnace, and then the high temperature diffusion experiment at 650°C was performed. Figure 1a shows the experimental schematic diagram of the diffusion process of G400, G450 and G500 in iodine vapor at 650°C for 96 h. And Figure 1b shows a schematic diagram of the experimental process of isothermal annealing of G400, G450 and G500 graphite loaded with iodine for 48 h. It is noteworthy that the isothermal annealing process was performed after the micro/nano-porous graphite had diffused in iodine vapor for 96 h and the iodine-loaded micro/nano-porous graphite was re-encapsulated in a quartz tube. The purpose of isothermal annealing is to study the process of iodine desorption and diffusion. Graphite samples were obtained by the diffusion process described above.

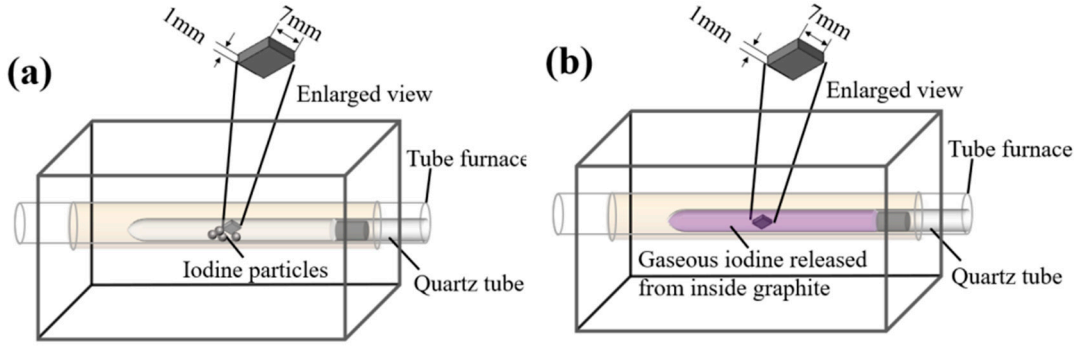

Figure 1. Schematic diagram of iodine diffusion experiments: (a) diffusion of micro/nano-porous graphite in iodine vapor at 650°C for 96 h; (b) isothermal annealing of iodine-loaded micro/nano-porous graphite for 48 h.

2.3. Characterizations

The morphology and structure changes of the graphite samples were monitored using SEM (LEO 1530VP) and their structures before and after iodine diffusion were measured using Bruker D8 Advance XRD with CuKα1 radiation source (λ=1.5406 Å). The radiation source is conditioned by two 2.5° Soller slits and a 0.025 mm Ni mask. Rutherford scattering spectrometry (RBS) was used to test the depth of diffusion of iodine in micro/nano-porous graphite by a Van de Graaff accelerator and a 2.0 Mev He^+ beam. The angle of incidence of helium ions is 165° and the spot of the test element signal is 1μm. The reflected X-ray intensities were collected by a LynxEye XE counter using continuous theta-2theta scans at a tube power of 40 kV/40 mA, ranging from 10° to 90° (2theta) with steps of 0.02° (2theta) at 0.15 s intervals. Changes in defects caused by iodine diffusion were recorded using a Raman spectrometer (XploRA INV, France) at an excitation wavelength of 473 nm and an effective penetration depth of about 50 nm. In addition, the abbreviations involved in the experiment are shown in Table 2.

Table 2. Description of the samples of experimental conditions.

Samples	Experimental conditions
G400	Pristine nanoporous graphite
G400-D96	Iodine diffusion in G400 at 650°C for 96 h

Preprints (www.preprints.org) | NOT PEER-REVIEWED | Posted: 19 July 2023 doi:10.20944/preprints202307.1246.v1

G400-H48	Isothermal annealing of G400 loaded with iodine for 48 h
G450	Pristine nanoporous graphite
G450-D96	Iodine diffusion in G450 at 650°C for 96 h
G450-H48	Isothermal annealing of G450 loaded with iodine for 48 h
G500	Pristine microporous graphite
G500-D96	Iodine diffusion in G500 at 650°C for 96 h
G500-H48	Isothermal annealing of G500 loaded with iodine for 48 h

3. Results and discussion

3.1. Microstructure

The porous microstructure of graphite consists of cracks, open and closed pores, and grain boundaries at a macroscopic scale. Figure 2(a-c) show the surface structure of micro/nano-porous graphite before iodine diffusion. Nanoporous graphite G400 and G450 have a smoother surface structure than microporous graphite G500, while the surface structure of G450 is more perfect than that of G400. Figure 2(d–f) shows the SEM images of graphite surfaces of G400, G450, and G500 diffused in iodine vapor at 650°C for 96 h. Compared with the microscopic morphology of the graphite surface in the original state, the surface of the diffused graphite becomes rougher. But the surface texture of G450 graphite is not as clear as that of G400 and G500, because G450 graphite is least affected by iodine vapor (G450 has the smallest average pore size). Figure 2(g–i) shows iodine-loaded micro/nano-porous graphite undergoing isothermal annealing for 48 h at the same temperature and vacuum to observe the diffusion of iodine from the inside of the graphite to the surface. Interestingly, iodine was precipitated near the pores on the surface of graphite after the annealed graphite stood at room temperature for a period of time, which indicates that pores are an important channel for graphite diffusion.

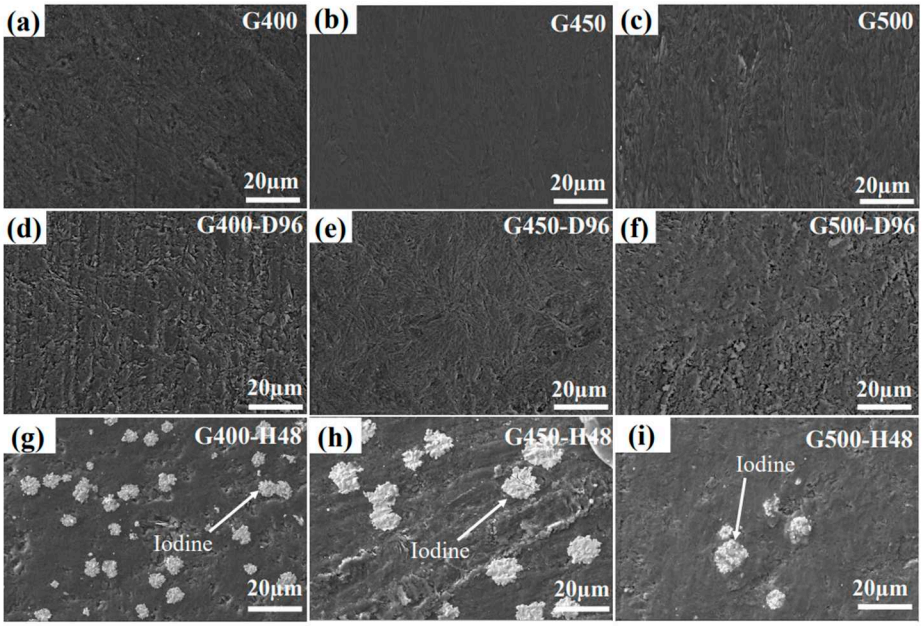

Figure 2. Surface SEM micrographs of micro/nano-porous graphite before and after iodine diffusion.

Random cracks and pores could be identified in the micro/nano-porous graphite of the pristine structure as shown in Figure 3. Figure 3a and 3b show large longitudinal pores inside G400, which are generated by the interaction between volatile gas escape during graphitization and anisotropic contraction of graphite crystals during the cooling phase of graphite manufacturing. Compared with

Preprints (www.preprints.org) | NOT PEER-REVIEWED | Posted: 19 July 2023 doi:10.20944/preprints202307.1246.v1

G400 and G500, nanoporous graphite G450 has a smooth surface and small pore size. However, G450's surface occasionally has scaly transverse pores. The pores on the surface of G500 are large and uniform, and these pores are caused by volatiles in the adhesive during the sintering process.

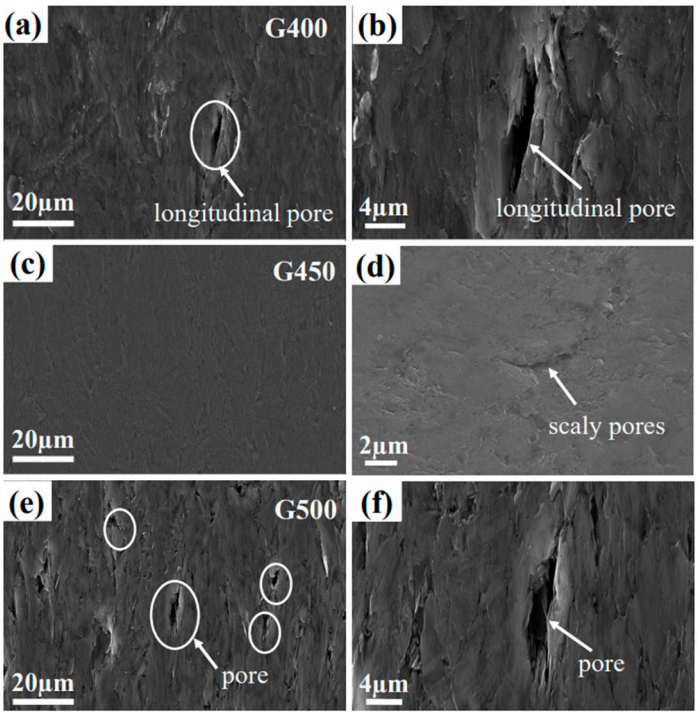

Figure 3. SEM micrographs of pores on the surface of G400, G450 and G500 graphite.

Figure 4 shows the EDS image of G400, G450 and G500 graphite diffused in iodine vapor for 96 h at 650 °C, respectively. The distribution of iodine diffusion is on the graphite surface, and the blues and reds in Figure 3 (b-c, e-f, and h-i) represent carbon and iodine, respectively. The relative content of iodine in G400, G450 and G500 are the same as that of energy dispersive spectrometer (EDS) analysis, as shown in Table 3. Since the diffusion of gaseous substances generally includes two processes of adsorption and diffusion, the smooth graphite surface is not easy to adsorb and diffuse substances. Iodine vapor is not easily attached to the smooth G450 graphite surface, so the iodine content on the surface of G450 is smaller than that of G400 and G500.

Table 3. The relative content of iodine and carbon on the surface of micro/nano-porous graphite after diffusion experiment.

Element	G400-D96	G450-D96	G500-D96
Carbon (%)	96.70 ±0.02	97.20 ±0.02	96.10 ±0.02
Iodine (%)	3.30 ±0.02	2.80 ±0.02	3.90 ±0.02

Preprints (www.preprints.org) | NOT PEER-REVIEWED | Posted: 19 July 2023 doi:10.20944/preprints202307.1246.v1

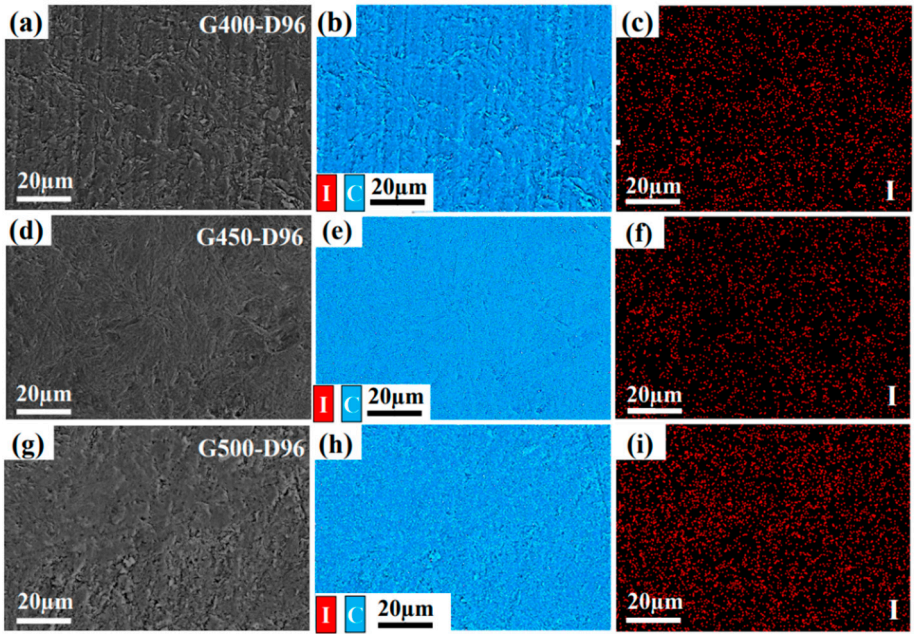

Figure 4. (Color online) Iodine distribution on the surface of G400, G450 and G500 graphite were respectively diffused in iodine vapor at 650°C for 96 h. a, d and g are the SEM image, and b-c , e-f and h-i are EDS image (blue and red color represent the distribution of C and I, respectively).

3.2. Rutherford backscattering spectrometry analysis

Rutherford backscattering spectrometry (RBS) is an efficient analytical method for detecting the diffusion depth of elements with higher atomic numbers in the periodic table in a matrix material for elements with lower atomic numbers [15, 16]. Figure 5a shows the RBS experimental spectra of micro/nano-porous graphite (G400, G450, and G500) after diffusion in iodine vapor at 650 °C for 96 h. The respective surface channel positions of C and I are indicated by arrows, and the distribution of I presents a distribution in which the concentration gradually decreases from the surface to the interior. Figure 5b shows the depth profiles of micro/nano-porous graphite (G400, G450, and G500) after diffusion in iodine vapor at 650 °C for 96 h. The difference in iodine distribution between nanoporous graphite G400 and G450 and microporous graphite G500 is shown in Figure 5a and 5b. The RBS experimental spectrum shows that after diffusing in iodine vapor at 650 °C for 96 h, the iodine content of G450 and G500 gradually decreases from the graphite surface to the interior of the matrix, while the iodine content of G400 has little difference between the surface and interior of graphite. The iodine content on the surface of G450 is higher than that of G400 and G500, which seems to be contradicted by the EDS analysis results that the iodine content on the surface of G450 is the least. The implementation is just the opposite, since the diffusion of gaseous species is related to the pore size and cracks of graphite. Nanoporous graphite G450 has a smaller average pore size, less defects such as cracks, and its surface is smooth. Although G400 graphite is also nanoporous graphite (average pore size is 23nm), its surface has cracks and large longitudinal pores. These larger cracks and longitudinal pores make the connected pore network on the surface of G400 larger (17.8% open porosity), resulting in little difference between its surface and internal iodine. These data results indicate that larger cracks and longitudinal pores propagate more easily. Both G450 and G500 graphite have a common point that the pore distribution is relatively uniform. The difference is that the open porosity of G450 (17.3%) is higher than that of G500 (12.8%),while the average pore diameter of G500 (553nm) is bigger than that of G450 (18nm). It can be seen from Figure 5a and 5b that there is more iodine on the surface of nanoporous graphite G450 with a depth of less than 400nm than that of G500, because the graphite surface with a larger open porosity is more likely to capture iodine. But at depths greater than 400 nm, the iodine distribution of both nanoporous graphite G400 and G450 are lower than that of microporous graphite G500. The iodine distribution of G450 graphite is the smallest of the three graphite, which is caused by its smaller average pore size and fewer frontal

Preprints (www.preprints.org) | NOT PEER-REVIEWED | Posted: 19 July 2023 doi:10.20944/preprints202307.1246.v1

defects. In short, nanoporous graphite G450 has better performance of blocking iodine diffusion in the process of adsorption and diffusion.

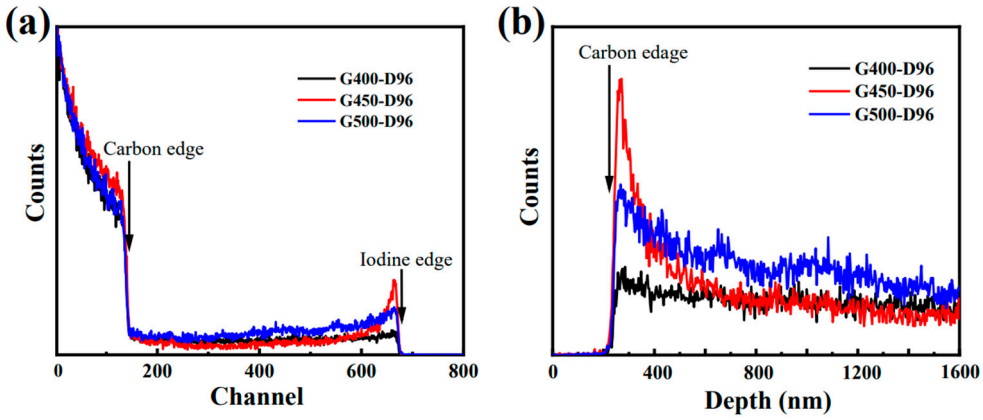

Figure 5. (a) RBS spectrum of iodine diffused in micro/nano-porous graphite at 650℃ for 96 h. (b) RBS depth profile of iodine diffused at 650℃ for 96 h.

Figure 6a shows the experimental RBS spectra of iodine-loaded micro/nano-porous graphite (G400, G450 and G500) annealed for 48 h under vacuum at 650°C to describe the desorption and diffusion behavior of iodine-loaded graphite. Figure 6b shows the depth distribution of iodine, and the surface of C is marked with arrows. Annealing causes iodine to diffuse deeper into the graphite. Since part of the iodine on the graphite surface is rapidly released during annealing, and the internal iodine continues to diffuse to the surface, a wide iodine peak appears in all three graphites at 650nm from the graphite surface. However, the iodine peak of microporous graphite G500 at 650 nm is not pronounced due to the formation of a stable iodine diffusion channel inside the G500 of the larger pore [17,18]. At depths greater than 1.4 μm, nanoporous graphite G400 and G450 have less iodine than microporous graphite G500, indicating that pore size is a key factor affecting iodine diffusion performance, and nanoporous graphite has better performance in blocking iodine diffusion than microporous graphite. Combined with the results of SEM surface morphology analysis, the nanoporous graphite G450 has the best performance in blocking iodine diffusion owing to smaller pores, fewer cracks and smoother surface.

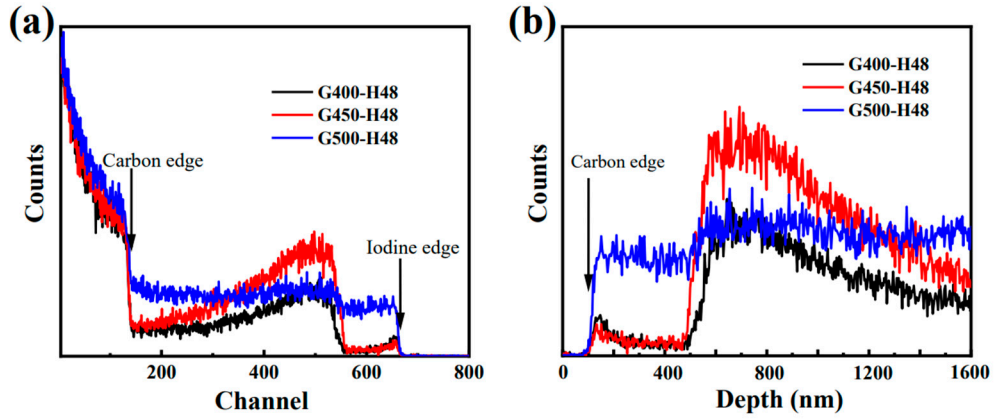

Figure 6. (a) RBS spectrum of iodine desorbed in micro/nano-porous graphite at 650°C for 48 h; (b) RBS depth profile of iodine desorbed at 650°C for 48 h.

3.3. Crystal structure

In order to illustrate the effect of iodine diffusion on graphite microstructure, the diffraction angle of (002) peak and Bragg formula were used to analyze the variation of graphite interlayer spacing. According to the Bragg formula $2d\sin\theta=n\lambda$ and $d_c=(d-d_1)/d$ (where d_c is the change in

Preprints (www.preprints.org) | NOT PEER-REVIEWED | Posted: 19 July 2023 doi:10.20944/preprints202307.1246.v1

interlayer spacing, d is the interlayer spacing of the original graphite, and d_1 is the graphite interlayer spacing after iodine diffusion) to calculate the graphite interlayer spacing before and after diffusion amount of change. Figure 7(a-c) show the X-ray diffraction (XRD) patterns of micro/nano-porous graphite (G400, G450 and G500) of different experimental conditions, including the change trend of micro/nano-porous graphite (002) peak, and the change trend of micro/nano-porous graphite interlayer spacing under different treatment time, respectively. Figure 7a shows that the (111) peak near the (002) peak indicated the iodine diffuses into micro/nano-porous graphite at 650°C, which is similar to the peaks that appear near the (002) peak of graphite in the literature due to the presence of silicon impurities [19, 20].

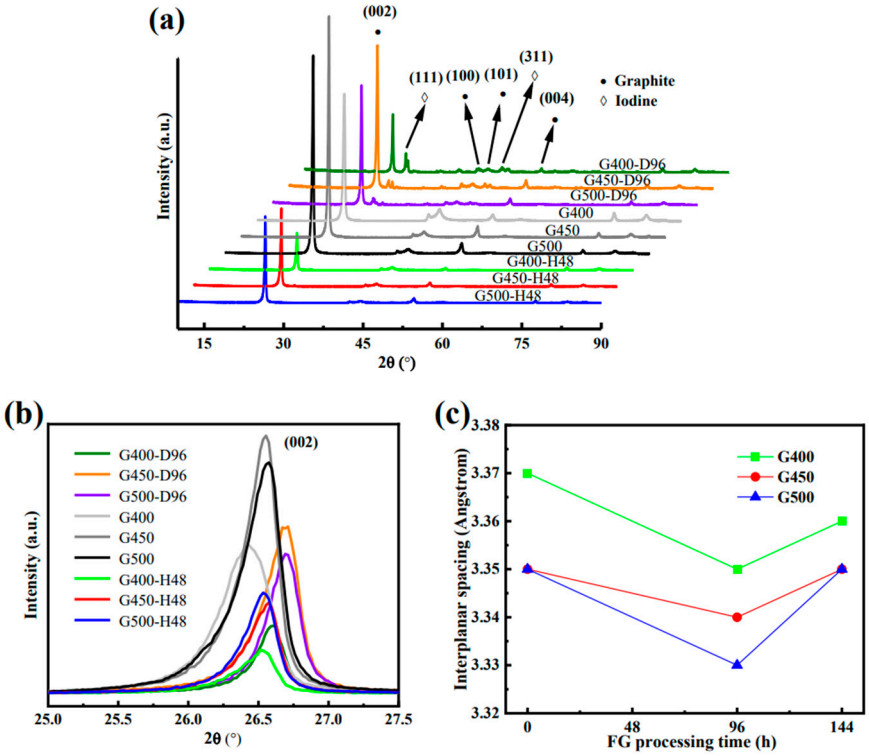

Figure 7. (a) XRD patterns of different experimental conditions, (b) The change trend of (002) peak, (c) The change trend of layer spacing of different experimental conditions.

Figure 7(a-b) shows the XRD spectra of microporous graphite, adsorption diffusion and isothermal annealing processes in the original state, and the presence of (111) peaks is thought to be related to iodine diffusion. Figure 7c shows graphite layer spacing vs. iodine diffusion. With the diffusion of iodine into graphite, the interlayer spacing of graphite decreases, while after iodine diffuses from graphite, the interlayer spacing of graphite tends to recover. This recoverable process is more like a physical reversible process. The decrease in the spacing of graphite layers is considered to be the internal stress caused by the diffusion of iodine and the mutual extrusion between graphite layers. However, the mechanism of their internal stress interaction needs further study. The abscissa of 144 h in Figure 7c is derived from the addition of two times, including the graphite sample first subjected to a 96-h iodine diffusion experiment and 48-h vacuum annealing experiment. The diffraction angle of d_{002} increased by 2θ due to iodine diffusion into graphite samples. But when iodine diffuses out during annealing, d_{002} seems to return to its initial state, which may be that iodine diffusion into the graphite grain boundary causes the graphite crystal to shrink along the c-axis. However, the shrinkage caused by diffusion is small (as iodine diffuses into graphite, the interlaminar spacing of nanoporous graphite G400 and G450 decreases by 5.9‰ and 2.9‰, respectively, and the interlaminar spacing of microporous graphite G500 decreases by 6.0‰) and can be restored. During the vacuum isothermal annealing process, the iodine on the graphite surface diffuses out, and the interlayer spacing of graphite returns to its original state because it is no longer

Preprints (www.preprints.org) | NOT PEER-REVIEWED | Posted: 19 July 2023 doi:10.20944/preprints202307.1246.v1

squeezed. These data indicate that iodine diffuses at high temperature with little energy and the effect on graphite crystals is recoverable [13]. The smaller the change in the spacing of graphite layers, the less affected the graphite structure is affected by iodine diffusion. The layer spacing change of nanoporous graphite is smaller than that of microporous graphite, which can effectively prevent the diffusion of iodine. The spacing change of the nanoporous graphite G450 layer was the smallest (2.9‰) by comparing the spacing changes of the three graphite layers. Nanoporous graphite G450 has the best effect of blocking iodine diffusion, which is consistent with the results of previous analyses.

Raman spectra of micro-nanoore graphite samples before and after the diffusion experiments were analyzed at a laser wavelength of 473 nm and an effective penetration depth of about 50 nm. The typical D and G characteristic bands of graphite were detected in the Raman band of 1300 cm^{-1} to 1700 cm^{-1} [14]. The position of the D peak signal in the Raman spectrum is independent of the defect type, and its appearance only requires the defect to participate in the phonon dispersion process to meet the momentum conservation law [15]. The pristine G400, G450 and G500 of the D and G peaks of the Raman spectra appear at about 1361 cm^{-1} and 1582 cm^{-1}, respectively. The D band strength I_D of graphite depends on the defect type and density. The strength ratio (I_D / I_G) of D band and G band are used to evaluate the grain size and graphitization degree [16]. Based on the integral area ratio between the D peak and G peak intensities, called I_D and I_G, respectively. The following equation was used to calculate the microcrystal size L_a [17]: $L_a\ (nm) = 2.4 \times 10^{-10} \lambda^4 \left(\frac{I_D}{I_G}\right)^{-1}$.

As shown in Table 4, the microcrystalline size L_a of micro/nano-porous graphite (G400, G450 and G500) decreases with iodine diffusion into this graphite. While L_a increases when iodine diffuses out of graphite (annealing process of iodine-loaded graphite). The decrease in the L_a value indicates that the graphite crystallites are subjected to extrusion forces in the a-axis, which is consistent with the result that the diffusion of iodine causes the graphite crystals to shrink along the c-axis by XRD patterns (Figure 7c). However, L_a is larger after annealing simply because the graphite microcrystals grow further after iodine diffusion out of the graphite. Usually, the relative intensity ratio of I_D/I_G is used to characterize the defect density of graphite [18]. The increase in I_D/I_G of micro/nano-porous graphite (G400, G450 and G500) after iodine diffusion is caused by the increase in defect density in graphite due to iodine diffusion. After annealing, the iodine escapes from the graphite matrix and the I_D/I_G of graphite decreases, indicating a decrease in defect density. Figure 8 shows that after 96 h of iodine diffusion at 650 °C, the position of D peak shifts to the left. The iodine diffused into the pores causes internal stress between the graphite flakes of graphite, which elastically deforms the graphite microcrystals. After annealing, the iodine diffuses out of the graphite matrix, and the position of the D peak is recovered due to the extrusion force of graphite microcrystals is weakened. These phenomena suggest that iodine diffusion affects the elastic or inelastic scattering of phonons, causing the movement of the D peak. The stocky Raman band between 500 cm^{-1} and 1300 cm^{-1} is considered a Raman characteristic peak of iodine vapor because this stocky peak disappears after annealing [27-29]. These data shown that the diffusion process of iodine only causes the deformation of graphite microcrystals without destroying the structure of graphite.

Table 4. Raman shifts of D and G peaks of graphite and the ratio of the intensity I_D/I_G.

Sample name	D peak wave number (cm^{-1})	G peak wave number (cm^{-1})	I_D/I_G (arbitrary units)	L_a (nm)
G400	1361	1583	0.34	35
G400-D96	1353	1582	0.39	31
G400-H48	1362	1582	0.28	43
G450	1362	1583	0.32	38
G450-D96	1356	1583	0.63	19
G450-H48	1362	1582	0.23	52
G500	1361	1581	0.32	38
G500-D96	1354	1583	0.38	32

Preprints (www.preprints.org) | NOT PEER-REVIEWED | Posted: 19 July 2023 doi:10.20944/preprints202307.1246.v1

G500-H48	1365	1583	0.20	60

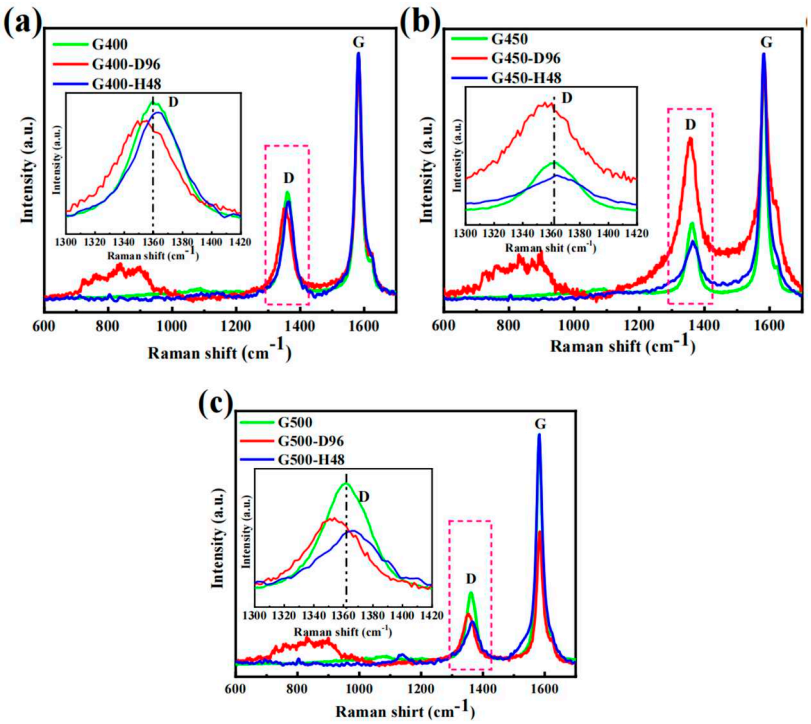

Figure 8. (a) Raman spectra of pristine, diffused and annealed nanoporous graphite G400 in the spectral range of 600–1700 cm^{-1}. (b) Raman spectra of pristine, diffused and annealed nanoporous graphite G450 in the spectral range of 600–1700 cm^{-1}. (c) Raman spectra of pristine, diffused and annealed microporous graphite G500 in the spectral range of 600–1700 cm^{-1}.

Figure 9 shows the Raman spectra yields of the D peak, D' peak and G peak. The D Peak (1361 cm^{-1}) is caused by the elastic scattering caused by the defect at the crystal boundary inside the graphite [22]. With the diffusion of iodine into and out of the graphite, the peak intensity ($I_{D'}$) of D' peak increased first and then decreased. The D' peak (1622 cm^{-1}) is relevant to the elastic scattering of vacancy defects near graphene [23]. The diffusion of iodine into the graphite led to the increase of the defect density. After the iodine diffuses into fine-grained graphite, the Raman curves show v peak (Figure 6a_1 and 6b_1). As the Ferrari's stated, the presence of the v peak is due to trans-polyacetylene in the grain boundary [30, 32]. The phenomenon of v peak after iodine diffusion due to the diffusion of iodine into the graphite grain boundary, which affects the trans-polyacetylene in the grain boundary. It is further explained that the changes caused by iodine diffusion for fine-grained graphite are physical processes and also reversible processes. And this is consistent with the previous discussion.

Preprints (www.preprints.org) | NOT PEER-REVIEWED | Posted: 19 July 2023 doi:10.20944/preprints202307.1246.v1

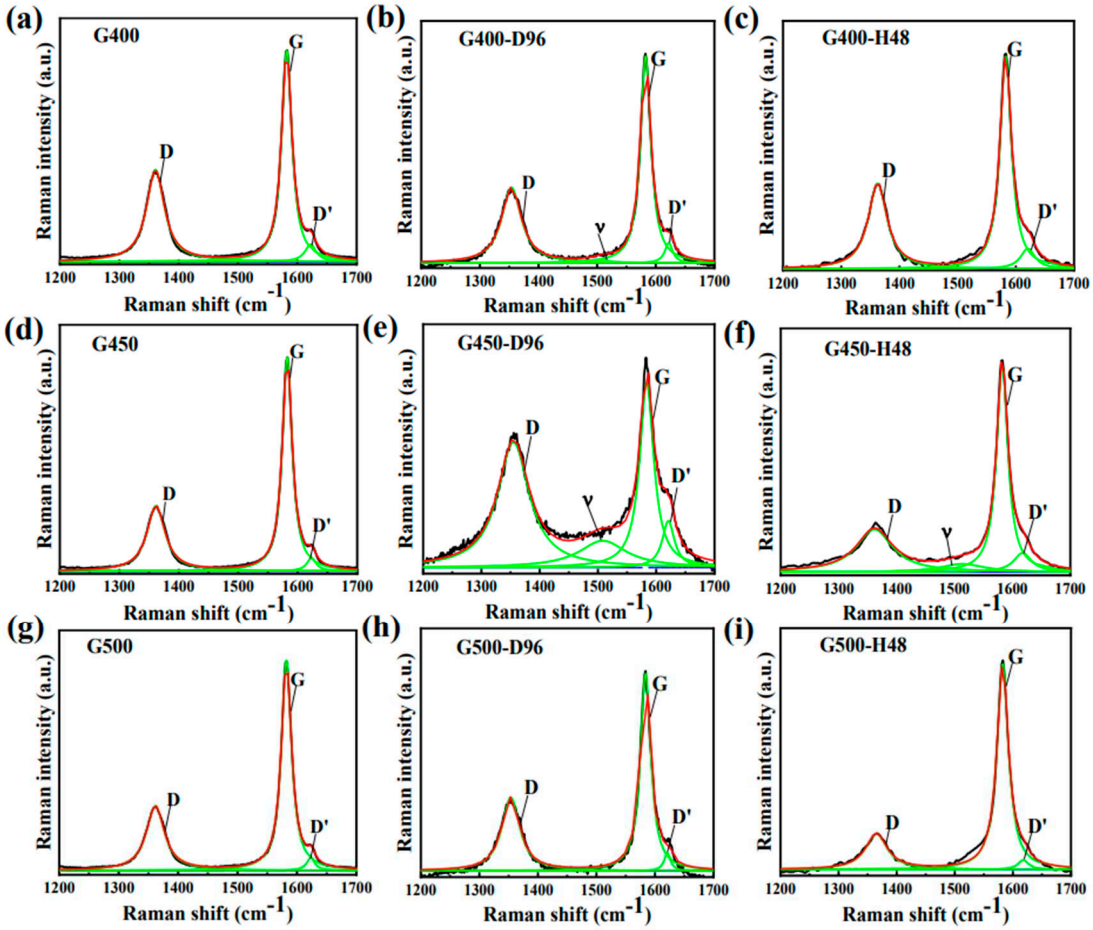

Figure 9. Raman spectra with linear background subtraction of (a-c) pristine fine-grained graphite (Containing the G400, G450 and G500), (a1-c1) iodine was diffused in fine-grained graphite at 650°C for 96 h and (a2-c2) fine-grained graphite containing iodine is held at 650°C for 48 h, all spectra were fitted with Lorentz line shape fitting.

3.4. Mechanistic analysis

Figure 10 shows a schematic diagram of the diffusion behavior of iodine in micro/nano-porous graphite at high temperature. This study finding that diffusion behavior of iodine in micro/nano-porous graphite is divided into three main aspects. First, iodine is captured by pores and microcracks at 650°C and diffuses into the graphite interior along the grain boundaries. Secondly, the iodine diffusing to the grain boundaries squeezes the graphite crystals along the c-axis and a-axis, leading to the reduction of layer spacing and L_a accompanied by the promotion of graphitization. Finally, when the graphite sample is isothermally annealed under vacuum conditions for 48 h, the iodine diffuses outward along the defects, the iodine content at the graphite grain boundaries decreases, and the squeezing force of the graphite crystals along the c-axis disappears. However, L_c increases with increasing holding time and the number of defects inside the graphite decreases. The iodine desorbed from the graphite surface evaporates into the environment with high temperatures.

Preprints (www.preprints.org) | NOT PEER-REVIEWED | Posted: 19 July 2023 doi:10.20944/preprints202307.1246.v1

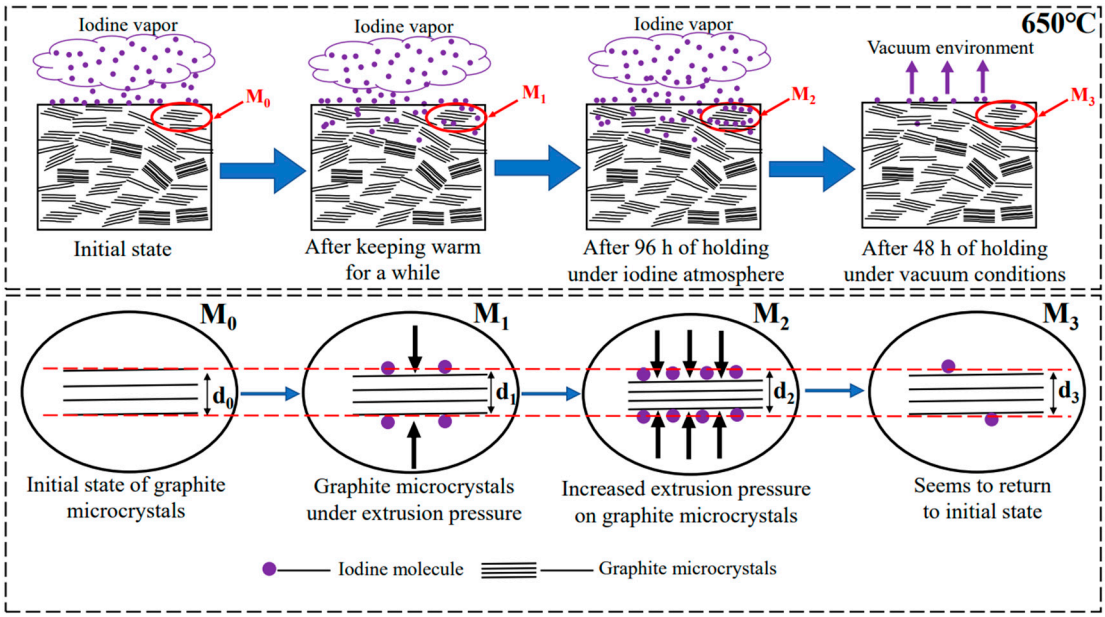

Figure 10. Schematic diagram of the diffusion behavior of iodine at high temperatures.

4. Conclusions

At 650°C, the diffusion depth of iodine in micro/nano-porous graphite G400, G450 and G500 was greater than 1.6 μm after 96 h of diffusion, and the iodine content in nanoporous graphite was lower than that in microporous graphite, indicating that nanoporous graphite could inhibit the diffusion of iodine better than microporous graphite. However, nanoporous graphite G450 is the best graphite among the three graphites in inhibiting the diffusion of gaseous iodine at high temperature due to its small pores, few defects and dense structure. The Raman spectroscopy and XRD results show that the diffusion of iodine causes the graphite microcrystals to shrink along the c-axis and a-axis, and the layer spacing of graphite decreases and the defect density increases; however, when iodine diffuses out of graphite, the layer spacing of graphite seems to return to the original state, and the defect density of graphite decreases, but the graphite microcrystal size (L_a) increases.

Acknowledgments: This work was financially supported by the National Natural Science Foundation of China (No. 52072397), DNL Cooperation Fund, CAS (DNL202012), the Top-notch Academic Programs Project of Jiangsu Higher Education Institutions (TAPP) and the partial research funding was from the Priority Academic Program Development of Jiangsu Higher Education Institutions (PAPD).

References

1. Mukhawana M B, Theron C C, Malherbe J B, et al. Behavior of iodine implanted in highly oriented pyrolytic graphite (HOPG) after heat treatment[J]. Nuclear Instruments and Methods in Physics Research Section B: Beam Interactions with Materials and Atoms, 2012, 273: 65-67.
2. Carter L M, Brockman J D, Robertdon J D, et al. ICP-MS measurement of iodine diffusion in IG-110 graphite for HTGR/ VHTR[J]. Journal of Nuclear Materials, 2016, 476: 30-35.
3. Verfondern K .Fuel performance and fission product behaviour in gas cooled reactors[J]. Iaea Tecdoc, 1997, pp. 448-453.
4. Müller A. Freisezung gasformiger Spaltproducte (Kr, Xe, J) aus Brennelmenten für Gasgekühlte Hochtemperaturreactoren, PhD thesis (Aachen), Jül 1295, Kernforschungsanlage, Jülich, 1976.
5. Carter L M, Brockman J D, Mater J D, et al. ICP-MS Measurement of cesium diffusion coefficients in NBG-18 graphite[J]. Journal of Nuclear Materials, 2015, 466: 402-408.
6. Carter L M, Brockman J D, Mater J D, et al. Diffusion of cesium and iodine in compressed IG-110 graphite compacts[J]. Journal of Nuclear Materials, 2016, 473: 218-222.
7. Adeojo S A, Malherbe J B, Njoroge E G, et al. Effect of sequential isochronal annealing on the structure and migration behaviour of selenium-ion implanted in glassy carbon[J]. Vacuum, 2020, 182: 109689.

8. Odutemowo O S, Marherbe J B, Theron C C. In-situ RBS studies of strontium implanted glassy carbon[J]. Vacuum, 2016, 126: 101-105.
9. Arregui-Mean J D, Worth R N, Bodel W, et al. Multiscale characterization and comparison of historical and modern nuclear graphite grades[J]. Materials Characterization, 2022, 190: 112047.
10. Hlatshwayo T T, Sebitla L D, Njoroge E G, et al. Annealing effects on the migration of ion-implanted cadmium in glassy carbon[J]. Nuclear Instruments and Methods in Physics Research Section B: Beam Interactions with Materials and Atoms, 2017, 395: 34-38.
11. Asthana A, Matsui Y, Yasuda M, Investigations on the structural disordering of neutron-irradiated highly oriented pyrolytic graphite by X-ray diffraction and electron microscopy[J]. Applied Crystallography, 2005, 38: 361-367.
12. Phillips R, Jolleya K, Zhou Y , et al. Influence of temperature and point defects on the X-ray diffraction pattern of graphite[J]. Carbon Trends, 2021, 5: 100124.
13. Li K, Liu Q, Cheng H, et al. Classification and carbon structural transformation from anthracite to natural coaly graphite by XRD, Raman spectroscopy, and HRTEM[J]. Spectrochimica Acta Part A: Molecular and Biomolecular Spectroscopy, 2021, 249: 119286.
14. Inam A, Brydson R, Edmonds D V. Raman spectroscopy study of the crystallinity of graphite formed in an experimental free-machining steel[J]. Materials Characterization, 2020, 163: 110264-110269.
15. Abbas G, Sonia F G, Zafar Z A, et al. Influence of structural properties on (de-)intercalation of ClO_4^- anion in graphite from concentrated aqueous electrolyte[J]. Carbon, 2022, 186: 612-623.
16. Que L K, Ai J P, Shao T H, et al. Fluorinated graphene films for ultra-high sensitivity of surface-enhanced Raman scattering[J]. Applied Surface Science, 2023, 616: 156496.
17. Zhang H Y, Lei Q T, Song J L, et al. Direct characterization of ion implanted nanoporous pyrolytic graphite coatings for molten salt nuclear reactors[J]. RSC Advances, 2018, 59: 33927-33938.
18. Schito A, Muirhead D K, Parnell J. Towards a kerogen-to-graphite kinetic model by means of Raman spectroscopy[J]. Earth-Science Reviews, 2023, 237: 104292.
19. Nakashima S, Norimoto M, Harima H. Raman scattering of iodine intercalated C_{60} crystals[J]. Chemical Physics Letters, 1997, 268: 359-364.
20. Chen S, Yuan Y, Yang X. In situ low-temperature Raman studies of iodine molecules confined in the one-dimensional channels of $AlPO_4$-5 crystals[J]. Microporous and Mesoporous Materials, 2016, 221: 76-80.
21. Congeduti A, Nardone M, Postorino P. Polarized Raman spectra of a single crystal of iodine[J]. Chemical Physics, 2000, 256: 117-123.
22. Liu M, Zhang W T, Song J L, et al. Irradiation resistance study of binderless nanoporous-isotropic graphite for use in molten salt nuclear reactors[J]. Nuclear Engineering and Design, 2018, 335: 231-240.
23. Li J Q, Qin Y, Chen Y L, et al. Structural characteristics and evolution of meta-anthracite to coaly graphite: A quantitative investigation using X-ray diffraction, Raman spectroscopy, and high-resolution transmission electron microscopy[J]. Fuel, 2023, 333: 126334.
24. Ferrari A C, Roberston J. Original of the 1150 cm^{-1} Raman mode in nanocrystalline diamond[J]. Physical Review B, 2001, 63: 121405.